Lipid Microdomains: Structural Correlations, Fluctuations, and Formation Mechanisms

Jun Fan
Department of Mechanical and Aerospace Engineering, Princeton University, Princeton, New Jersey 08544, USA

Maria Sammalkorpi*
Department of Mechanical and Aerospace Engineering, Princeton University, Princeton, New Jersey 08544, USA

Mikko Haataja
Department of Mechanical and Aerospace Engineering, Princeton Institute for the Science and Technology of Materials (PRISM), Program in Applied and Computational Mathematics (PACM), Princeton University, Princeton, New Jersey 08544, USA
(Received 1 December 2009; published 17 March 2010)

Compositional lipid microdomains (''lipid rafts'') in mammalian plasma membranes are believed to facilitate many important cellular processes. While several physically distinct scenarios predicting the presence of finite-sized microdomains *in vivo* have been proposed in the past, direct experimental verification or falsification of model predictions has remained elusive. Herein, we demonstrate that the combination of the spatial correlation and temporal fluctuation spectra of the lipid domains can be employed to unambiguously differentiate between the existing theoretical scenarios. Furthermore, the differentiation of the raft formation mechanisms using this methodology can be achieved by collecting data at physiologically relevant conditions without the need to tune control parameters.

DOI: 10.1103/PhysRevLett.104.118101 PACS numbers: 87.14.Cc, 87.15.A−, 87.16.D−

The plasma membrane (PM) enveloping mammalian cells is a bilayer consisting of thousands of different types of lipids and proteins. Far from being featureless, it is now well established that the membrane is ''patchy'' with spatially organized regions of structure and function, both in terms of lipids and proteins; for an overview, see Ref. [1]. In particular, the outer leaflet of the PM contains compositional microdomains called *lipid rafts* enriched in saturated lipids and cholesterol; these domains are associated with increased levels of lipid translational and conformational order, and are believed to participate in the control of transmembrane signal transduction, membrane trafficking, cytoskeletal composition, and viral budding [2–5]. Experiments suggest that the rafts have a typical size $\sim$20–200 nm with estimated lifetimes ranging from $\sim 10^{-3}$ s [6] to 10^{2} s [7]. Very recently, advances in experimental techniques have enabled *in vivo* imaging of single diffusing lipid molecules and proteins with unprecedented spatial resolution within the membrane [8]; the physical picture emerging is that of local ''trapping'' of raft-associated lipids and proteins by microdomains with typical trapping times $\sim 10^{-2}$ s and spatial confinement in regions of $\sim$20 nm in linear dimension.

Given the biophysical and chemical complexity of the plasma membrane, the fundamental challenge is to infer the raft domain formation and regulation mechanism(s) from experimental data. Indeed, from a broader biophysical perspective, resolving the actual formation mechanism is critical as this would provide novel insight into the cell's ability to regulate the size, lifetime, and spatial localization of the domains. While several theoretical models have been developed to explain the presence of finite-sized lipid microdomains, the biophysical mechanisms responsible for raft formation and regulation have remained elusive. Some have argued that the presence of these domains *in vivo* is a property of the membrane in thermal equilibrium [9,10], while others have invoked nonequilibrium, cellular lipid transport processes [11–15]. In the equilibrium case, the raft domains have been suggested to either result from (I) critical fluctuations associated with a nearby critical point at $T = T_c$ [9] or (II) pinning of compositional interfaces by immobile membrane proteins [10]. In the nonequilibrium case, stochastic lipid transport to and from the membrane (''lipid recycling'') has been singled out as a possible mechanism for supporting finite-sized domains in both (III) miscible [11] and (IV) immiscible [12,13] lipid systems, while (V) coupling the membrane to a lipid reservoir at $T < T_c$ has also been shown to result in finite-sized domains [14,15]. Henceforth, the numbering I–V will be employed to refer to these scenarios. A very recent review on the theoretical models for raft formation can be found in Ref. [16].

Now, given the broad range of physical mechanisms incorporated in the aforementioned theoretical models, it is conceivable that the spatiotemporal behavior of the lipid composition may provide important clues as to which of the mechanisms is the dominant one. Indeed, in this Letter, we demonstrate that the structure of microdomains and their relaxation times can be exploited as ''fingerprints'' of their formation mechanism. More specifically, we show that spatiotemporal correlations in the lipid composition field possess distinct features specific to the formation

mechanism under consideration, thereby providing a means to resolve this long-standing problem in the field of membrane biophysics. We next demonstrate the feasibility of this approach by extracting the spatiotemporal correlations from simulations of the existing theoretical models (I–V) within the modeling approach introduced in our earlier work [13].

Model equations.—Our starting point is a (dimensionless) stochastic, nonlinear reaction-diffusion equation for $c(\mathbf{r}, \tau)$, the deviation of the local composition from the critical composition within the outer leaflet, which incorporates the presence of critical fluctuations [9], interface pinning by immobile membrane proteins [10], nonequilibrium recycling processes [11,13], and the presence of a lipid reservoir [14,15]:

$$\frac{\partial c(\mathbf{r}, \tau)}{\partial \tau} = -\frac{1}{\tau_r}(c - \bar{c}) + M\nabla^2 \frac{\delta \mathcal{F}}{\delta c} + \eta(\mathbf{r}, \tau), \qquad (1)$$

where $\mathcal{F} = \int d\mathbf{r}\{W^2/2[1 - \alpha\rho(\mathbf{r})](\nabla c)^2 + \Lambda c^2/2 + c^4/4\}$ denotes the free energy of the effectively binary lipid system, M is the mobility, τ_r denotes a relaxation time due to coupling to a lipid reservoir [14,15], $\bar{c}$ denotes the average composition imposed by the reservoir, and η denotes a stochastic Gaussian noise term with mean $\langle\eta\rangle = 0$ and correlator $\langle\eta(\mathbf{r}, \tau_1)\eta(\mathbf{r}', \tau_2)\rangle = -H^2/(2\pi)\nabla^2 K_0(|\mathbf{r} - \mathbf{r}'|/\ell)\delta(\tau_1 - \tau_2)$ [13]. The parameter H can be related to either the temperature of the system or the rate at which lipids are removed and added to the leaflet due to vesicular and nonvesicular lipid trafficking events, while ℓ denotes the recycling length over which spatial redistribution of lipids takes place [13]. Furthermore, $K_0(x)$ is a modified Bessel function of the second kind of the zeroth order, $\rho(\mathbf{r}) = \pi\sigma^{-2}\sum_i^N \exp(-|\mathbf{r} - \mathbf{r}_i|^2/2\sigma^2)$ denotes the local concentration of N immobile membrane proteins of typical linear dimension σ, W is a parameter which controls the line tension between the raft and nonraft phases, and $\alpha > 0$ is a parameter which accounts for the local reduction in the line tension due to immobile membrane proteins [17] and leads to interface pinning. Also, $c < 0$ ($c > 0$) is taken to represent the raft (nonraft) phase, while in Eq. (1), the parameter $\Lambda > 0$ ($\Lambda < 0$) is appropriate for $T > T_c$ ($T < T_c$). Finally, equilibrium fluctuations are obtained when $\ell \lesssim \xi$, where ξ denotes the static correlation length, while nonequilibrium stochastic recycling corresponds to $\ell \gg \xi$ [13,16]. We note that the formulation of the model equations as in Eq. (1) is convenient in that while it incorporates all of the physical mechanisms discussed above, the distinct mechanisms can be investigated separately by making specific choices for the model parameters.

Numerical simulations.—The specific choices for the parameters (τ_r, Λ, ℓ, H, α, N) employed in the simulations for scenarios I–V are listed in Table I; quantitatively similar behavior is found for a broad range of parameter values. The remaining four parameters $\bar{c}$, M, σ, and W were set to $\bar{c} = 0.3$, $M = 1$, $\sigma = 1/\sqrt{2}$, and $W = 1$ in all simulations reported here. For the numerics, finite-differencing was adopted for both spatial and temporal derivatives in the discretized version of Eq. (1). The system size is $L \times L$, where $L = 256$ with periodic boundary conditions; the results discussed in this Letter did not display any detectable finite-size effects. Converting to physical quantities, dimensionless length and time scales correspond to 1 nm and 10^{-5} s, respectively [13]. The initial compositions were given small-amplitude random fluctuations with $\int_{\mathbf{r}} c(\mathbf{r}, 0) = 0$, corresponding to the critical composition. Dimensionless time step $\Delta\tau = 0.005$ and grid spacing $\Delta x = 1$ were employed in all simulations; we verified that the simulation results have converged with respect to both of these choices. Finally, the noise term was constructed in Fourier representation.

Spatial fluctuations and temporal correlations.—A very useful way of extracting quantitative data from the spatiotemporal dynamics of $c(\mathbf{r}, \tau)$ is provided by the so-called speckled scattering intensity and its correlations [18–21]. Following Ref. [19], we introduce the scattering intensity $I(\mathbf{q}, \tau) \equiv |\hat{c}(\mathbf{q}, \tau)|^2$ and the static structure factor $S(\mathbf{q}) = \langle I(\mathbf{q}, \tau)\rangle$, where $\langle ...\rangle$ denotes a temporal average under steady-state conditions, and $\hat{c}(\mathbf{q}, \tau) = \int d\mathbf{r} e^{i\mathbf{q}\cdot\mathbf{r}} c(\mathbf{r}, \tau)$. Of particular interest is the normalized steady-state intensity correlation function

$$\mathrm{Corr}(\mathbf{q}, \tau) = \frac{\langle I(\mathbf{q}, \tau_1) I(\mathbf{q}, \tau_1 + \tau)\rangle - \langle I(\mathbf{q}, \tau_1)\rangle^2}{\langle I^2(\mathbf{q}, \tau_1)\rangle - \langle I(\mathbf{q}, \tau_1)\rangle^2}, \qquad (2)$$

which equals unity at $\tau = 0$ and typically decays to zero exponentially at large τ with a characteristic wave-vector dependent relaxation time τ_q such that $\mathrm{Corr}(\mathbf{q}, \tau_q) = 1/e$. Figure 1 displays the spherically averaged $\mathrm{Corr}(\mathbf{q}, \tau)$ for the five scenarios obtained from simulations, as well as

TABLE I. Simulation parameters for the five scenarios. τ_r, Λ, ℓ, H, α, and N denote the relaxation time imposed by a lipid reservoir, deviation of the (dimensionless) temperature from the mean-field critical temperature, recycling length, recycling strength, protein-interface coupling term, and number of immobile membrane proteins, respectively.

Scenario	τ_r	Λ	ℓ	H	α	N
I–critical fluctuations	∞	-0.001	0.1	0.0283	0	0
II–interface pinning by proteins	∞	-1	1	0.85	$1/\pi$	1500
III–recycling in miscible system	∞	10	1280	0.85	0	0
IV–recycling in immiscible system	∞	-1	1280	0.85	0	0
V–coupling to lipid reservoir	500	-1	0.1	2.12	0	0

TABLE II. Behavior of the structure factor $S(\mathbf{q})$ and correlation function $\mathrm{Corr}(\mathbf{q}, \tau)$ for different theoretical raft formation scenarios.

Raft formation scenario	$S(\mathbf{q})$	$\mathrm{Corr}(\mathbf{q}, \tau)$
I–critical fluctuations	$\sim[1 + (q\xi)^{7/4}]^{-1}$	$\sim \exp[-\tau/\tau_q]$; $\tau_q^{-1} \sim q^2\xi^2(1 + q^{7/4}\xi^{7/4})$
II–interface pinning by proteins	$\sim q^{-3}$	$\sim \exp[-C(\ln\tau)^2]$
III–recycling in miscible system	$\sim q^{-2}$	$\sim \exp[-\tau/\tau_q]$; $\tau_q^{-1} \sim q^2$
IV–recycling in immiscible system	$\sim[q^2(1 + Bq)]^{-1}$	$\sim \exp[-\tau/\tau_q]$; $\tau_q^{-1} \sim q^2(1 + Aq^2)$
V–coupling to lipid reservoir	sharply peaked	$\sim \exp[-\tau/\tau_q]$; $\tau_q \to \infty$ at several q

representative snapshots. Not surprisingly, the data clearly reveal that long wavelength fluctuations decay more slowly than the short wavelength ones in cases I–IV. Also, note that while the characteristic relaxation times for scenarios I and IV are similar in magnitude, the behavior for scenario II is strikingly different: short wavelength fluctuations relax on the same time scale as in scenarios I and IV, while long wavelength fluctuations seemingly ''freeze in'' and have orders of magnitude longer effective relaxation times than in scenarios I, III, or IV. Finally, note the presence of an extended set of wave numbers at finite $\mathbf{q}$ which appear to remain frozen in scenario V.

Structure factor and relaxation time.—Next, we examine the behavior of the spherically averaged structure factor $S(\mathbf{q})$ and characteristic relaxation time τ_q, shown in Fig. 2, for the different scenarios. Regarding $S(\mathbf{q})$, it can be seen that scenarios I–IV are associated with scaling behavior at intermediate and/or large q. More specifically, $S(\mathbf{q}) \sim q^{-\alpha}$ where $\alpha \approx 2$ for scenarios I and III, while $\alpha \approx 3$ for scenarios II and IV at large q. The former behavior for scenario I is consistent with the expected critical structure factor for the 2D Ising model ($\sim q^{-7/4}$) [22], while the q^{-3} behavior for scenarios II and IV is due to the presence of sharp 1D interfaces in a 2D system (so-called Porod's law—see, e.g., Ref. [23]). Finally, for scenario V, $S(\mathbf{q})$ displays sharp maxima corresponding to the fundamental spatial periodicity of the pattern and its higher order harmonics.

Turning now to τ_q, for scenario I, $\tau_q \sim q^{-2}$ ($\sim q^{-15/4}$) when $q\xi \ll 1$ ($q\xi \gg 1$), as appropriate for Model B [22]. For scenarios III and IV, the data are well-described by $\tau_q \sim q^{-2}$ and $\tau_q \sim (q^2 + Aq^4)^{-1}$, respectively, where A denotes a constant. On the other hand, for scenario II, the data suggests that spatial fluctuations at long wavelengths decay anomalously slowly in this case due to the existence of large compositionally ordered domains in the so-called Griffiths phase [24], pinned by the immobile proteins. In particular, we expect that $\mathrm{Corr}^{(\mathrm{II})}(\mathbf{q}, \tau) \sim \exp[-C(\ln\tau)^2]$, where C is a constant, implying a diverging relaxation time at long wavelengths [25,26] consistent with our simulation data. Finally, for scenario V, the simulation data indicate that τ_q becomes very large for wave vectors corresponding to the fundamental spatial periodicity of the pattern and its higher order harmonics.

Discussion.—The behavior of the structure factors and intensity correlation functions for the five raft formation scenarios, summarized in Table II, constitute the central result of this Letter. Specifically, the analysis implies that the combination of spatial correlations and temporal fluctuation spectra of lipid microdomains can be employed to unambiguously distinguish between the different theoretical models experimentally, provided that the experiment probes a broad range of length scales with sufficient temporal resolution. In particular, the large $\mathbf{q}$ behavior of the structure factor can be employed to distinguish between systems above and below T_c [$S(\mathbf{q}) \sim q^{-2}$ for scenarios I/III

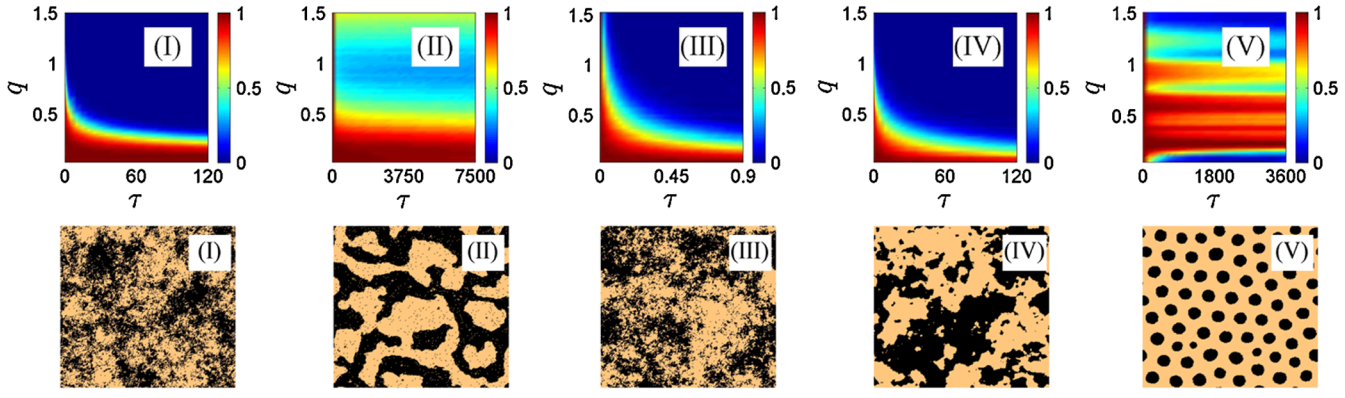

FIG. 1 (color online). Top row: Intensity correlation function $\mathrm{Corr}(\mathbf{q}, \tau)$ from Eq. (2) computed for the five scenarios (I–critical fluctuations; II–pinning of compositional interfaces by immobile membrane proteins; III–stochastic recycling above T_c; IV–stochastic recycling below T_c; and V–coupling to lipid reservoir). Bottom row: representative snapshots of raft (black) and nonraft (copper) microdomains. Note the formation of well-defined interfaces in scenarios II and IV, and the development of a spatially periodic structure in scenario V.

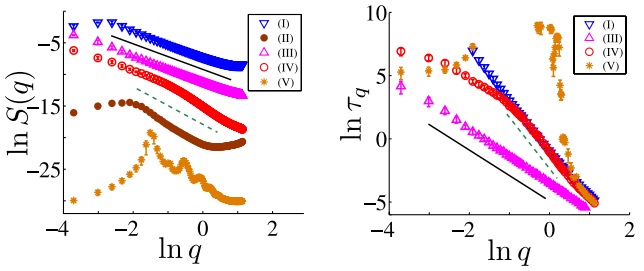

FIG. 2 (color online). Logarithmic behavior of the static structure factor $S(\mathbf{q})$ (left panel) and the characteristic relaxation time τ_q (right panel). Note that the data for $S(\mathbf{q})$ have been shifted vertically for clarity. In the left panel, the solid and dashed lines are guides to the eye, and have slopes -2 and -3, respectively, while in the right panel, the corresponding slopes are -2 and -4. Note that relaxation times are ill-defined at small q for scenario II and are thus excluded from the plot.

vs q^{-3} for II/IV vs sharply peaked for V], while temporal decay of correlations provides the means to further distinguish between scenarios II, IV, and V [$\tau_q \rightarrow \infty$ vs $\tau_q \sim q^{-2}$ vs sharply peaked]. Furthermore, scenarios I and III can be differentiated by noting that for scenario I, $S(\mathbf{q}) \sim$ Const. in the regime where the $\tau_q \sim q^{-2}$ scaling holds, while it continues to scale as q^{-2} for scenario III. We note that it has been proposed recently that the static structure factor can be exploited to distinguish between raft domain formation via critical fluctuations and microemulsions [27].

Of course, we cannot rule out the possibility that the operational raft formation mechanism does not correspond to any of the five proposed mechanisms, or that it is a combination of multiple concurrently operating ones. In the former case, experimentally obtained spatial correlation function and relaxation time data would place stringent physical and mathematical constraints on the next generation of theoretical models. In the latter case, on physical grounds one would expect recycling fluctuations to dominate over thermal fluctuations, and thus a combination of scenarios I and III would display fluctuation behavior appropriate for scenario III, while we expect the anomalous dynamics found in scenario II to dominate over the recycling dynamics in scenarios IV or V.

In conclusion, in this Letter, we have demonstrated that the combination of spatial correlations and temporal fluctuation spectra of lipid microdomains can be employed to unambiguously differentiate between the raft formation mechanisms that have been proposed in the past. It is important to note that the data only need to be collected at a fixed temperature, as the different theoretical models give rise to very different quantitative behavior as far as $S(\mathbf{q})$ and τ_q are concerned. Finally, we are currently developing hybrid particle-continuum simulation methods to investigate how to extract these correlations from, e.g., multiple-particle tracking experiments with submillisecond temporal and nanoscale spatial resolution.

This work has been in part supported by an NSF-DMR Grant No. DMR-0449184 and the NSF-MRSEC Program, Grant No. DMR-0213706 at Princeton University.

*Formerly M. Huhtala. Present address: Department of Chemical Engineering, Yale University, New Haven, CT 06520.

[1] D. M. Engelman, Nature (London) **438**, 578 (2005).
[2] D. A. Brown and E. London, Annu. Rev. Cell. Develop. Biol. **14**, 111 (1998).
[3] K. Simons and E. Ikonen, Nature (London) **387**, 569 (1997).
[4] M. Edidin, Annu. Rev. Biophys. Biomol. Struct. **32**, 257 (2003).
[5] J. F. Hancock, Nat. Rev. Mol. Cell Biol. **7**, 456 (2006).
[6] A. Kusumi, I. Koyama-Honda, and K. Suzuki, Traffic **5**, 213 (2004).
[7] A. Pralle, P. Keller, E. L. Florin, K. Simons, and J. K. H. Horber, J. Cell Biol. **148**, 997 (2000).
[8] C. Eggeling *et al.*, Nature (London) **457**, 1159 (2009).
[9] S. L. Veatch *et al.*, ACS Chem. Biol. **3**, 287 (2008).
[10] A. Yethiraj and J. C. Weisshaar, Biophys. J. **93**, 3113 (2007).
[11] L. A. Gheber and M. Edidin, Biophys. J. **77**, 3163 (1999).
[12] M. S. Turner, P. Sens, and N. D. Socci, Phys. Rev. Lett. **95**, 168301 (2005).
[13] J. Fan, M. Sammalkorpi, and M. Haataja, Phys. Rev. Lett. **100**, 178102 (2008); Phys. Rev. E **81**, 011908 (2010).
[14] L. Foret, Europhys. Lett. **71**, 508 (2005).
[15] J. Goméz, F. Sagués, and R. Reigada, Phys. Rev. E **77**, 021907 (2008); Phys. Rev. E **80**, 011920 (2009).
[16] J. Fan, M. Sammalkorpi, and M. Haataja, FEBS Lett. (to be published).
[17] M. Laradji, H. Guo, M. Grant, and M. J. Zuckermann, J. Phys. Condens. Matter **4**, 6715 (1992).
[18] S. Brauer *et al.*, Phys. Rev. Lett. **74**, 2010 (1995).
[19] G. Brown, P. A. Rikvold, M. Sutton, and M. Grant, Phys. Rev. E **56**, 6601 (1997).
[20] A. Fluerasu, M. Sutton, and E. M. Dufresne, Phys. Rev. Lett. **94**, 055501 (2005).
[21] M. Leitner *et al.*, Nature Mater. **8**, 717 (2009).
[22] P. C. Hohenberg and B. I. Halperin, Rev. Mod. Phys. **49**, 435 (1977).
[23] A. J. Bray, Adv. Phys. **51**, 481 (2002).
[24] R. B. Griffiths, Phys. Rev. Lett. **23**, 17 (1969).
[25] D. Dhar, M. Randeria, and J. P. Sethna, Europhys. Lett. **5**, 485 (1988).
[26] P. Calabrese, A. Pelissetto, and E. Vicari, Phys. Rev. E **77**, 021126 (2008).
[27] A. R. Hohnerkamp-Smith, S. L. Veatch, and S. L. Keller, Biochim. Biophys. Acta **1788**, 53 (2009).